

SOLVING THE OBLIQUE DERIVATIVE BOUNDARY-VALUE PROBLEM BY THE FINITE VOLUME METHOD*

MAREK MACÁK, KAROL MIKULA AND ZUZANA MINARECHOVÁ†

Abstract. This paper deals with the oblique derivative boundary-value problem and its solution by the finite volume method. In this approach, the oblique derivative in the boundary condition is decomposed into this normal and tangential components which are then approximated by means of numerical solution values. The appropriate numerical schemes for 2D and 3D domains are developed and numerical experiments are performed. The numerical solutions are compared to the exact solutions and the second order accuracy of our 2D and 3D numerical scheme is obtained in all experiments. Our work is motivated by the large scale oblique derivative boundary value problem of physical geodesy.

Key words. finite volume method, oblique derivative boundary-value problem

AMS subject classifications. 35J25, 65N08

1. Introduction. Let us consider the following oblique derivative boundary-value problem (BVP) in the bounded domain Ω :

$$-\Delta u(\mathbf{x}) = 0, \quad \mathbf{x} \in \Omega, \quad (1.1)$$

$$\langle \nabla u(\mathbf{x}), \vec{s}(\mathbf{x}) \rangle = p(\mathbf{x}), \quad \mathbf{x} \in \Gamma \subset \partial\Omega, \quad (1.2)$$

$$u(\mathbf{x}) = q(\mathbf{x}), \quad \mathbf{x} \in \partial\Omega - \Gamma, \quad (1.3)$$

where u represents the unknown potential function, (1.2) represents the oblique derivative boundary condition (BC) and \langle, \rangle denotes the inner product.

The BPV (1.1)-(1.3) represents a modification of the crucial problem of physical geodesy which is known as the fixed gravimetric BVP. In case of the fixed gravimetric BVP, the computational domain is unbounded and BVP is defined as follows, cf. [12, 8, 9, 3]:

$$-\Delta T(\mathbf{x}) = 0, \quad \mathbf{x} \in R^3 - S, \quad (1.4)$$

$$\langle \nabla T(\mathbf{x}), \vec{s}(\mathbf{x}) \rangle = -\delta g(\mathbf{x}), \quad \mathbf{x} \in \partial S, \quad (1.5)$$

$$T(\mathbf{x}) \rightarrow 0, \quad \text{as } |\mathbf{x}| \rightarrow \infty, \quad (1.6)$$

where, in this field of study, T is the so-called disturbing potential, S is the Earth's body, $\delta g(\mathbf{x})$ represents co-called gravity disturbance obtained by gravity measurements and $|\mathbf{x}| = (\sum_{i=1}^3 x_i^2)^{1/2}$. Since (1.4)-(1.6) is defined in the infinite domain, for solving this problem by finite volume method (FVM) we construct a bounded domain Ω in the external space above the Earth [6]. The bottom surface $\Gamma \subset \partial\Omega$ represents a part of the Earth surface ∂S . The upper spherical part and also further artificial planar boundaries of the bounded domain represents the additional boundary where the Dirichlet-type BC is prescribed. Such problem where we consider the oblique derivative BC on Γ and Dirichlet BC elsewhere corresponds to (1.1)-(1.3).

There exist several approaches to the solution of fixed gravimetric BVP in physical geodesy. For the global gravity field modelling mainly spherical harmonics are used

*This work was supported by Grant No.: VEGA 1/0269/09, APVV-0072-11

†Slovak University of Technology, Faculty of Civil Engineering, Radlinského 11, 813 68 Bratislava, Slovakia (macak@math.sk, mikula@math.sk, minarechova@math.sk).

and, for the local modelling the FFT-based methods [16] and the collocation [17] are performed. Recently, further numerical methods are applied to the problems of physical geodesy. The boundary element method (BEM) was used in [10, 11, 13, 3] and finite element method (FEM) and FVM were used in [14, 7, 6]. In these approaches, the oblique derivative problem was transformed to a standard Neumann BVP considering special projection of the oblique derivative to the normal of the Earth. To obtain a numerical solution of fixed gravimetric BVP, in which the oblique derivative is treated by its decomposition into normal and tangential components to the Earth's surface, the BEM and the collocation with linear basis functions were applied in [4]. The variational method based on a weak formulation of (1.4)-(1.6) was presented in [9].

Our aim is to present the novel scheme for solving oblique derivative BVP (1.1)-(1.3) by the FVM in 2D and 3D domains. Opposite to the previous FEM and FVM approaches, in this paper we decompose the oblique derivative to its normal and tangential components and tested FVM by using such approach. A 2D FVM for oblique derivative problems together with theoretical analysis was presented in [2]. In this paper we solve the oblique derivative BVP in circular and spherical domains and we show that experimental order of convergence (EOC) of the developed algorithms is equal to 2. In a near future, we believe that this algorithm will be successfully applied in solving the fixed gravimetric BVP with real gravimetric measurements on the real Earth surface.

2. Solution to the oblique derivative BVP by the finite volume method.

The FVM is based on the approximation of conservation laws. It can be used on arbitrary geometries, using structured or unstructured meshes, and it leads to robust numerical solution. In FVM approach, we divide the computational domain into a number of finite volumes p . Then, the integration over a finite volume and using divergence theorem

$$-\int_p \Delta u \, dx dy dz = -\int_{\partial p} \nabla u \cdot \vec{n} \, d\sigma, \quad (2.1)$$

yield the *weak formulation* of the equation (1.4) in the finite volume p

$$-\int_{\partial p} \frac{\partial u}{\partial \vec{n}} \, d\sigma = 0. \quad (2.2)$$

Let $q \in N(p)$ be a neighbour of finite volume p , where we have denoted by $N(p)$ all neighbours of p . Let u_p and u_q be approximate values of u in p and q , e_{pq} is a boundary of finite volume p common with q respectively, \vec{n}_{pq} is its unit normal vector oriented from p to q and must be satisfied that \vec{n}_{pq} is orthogonal to e_{pq} , $m(e_{pq})$ is the area of e_{pq} . Let x_p and x_q by representative points of p and q respectively (e.g. centers of gravity) and d_{pq} their distance. If we approximate the normal derivative along the boundary of finite volume p by

$$\frac{\partial u}{\partial n_{pq}} \approx \frac{u_q - u_p}{d_{pq}}, \quad (2.3)$$

we obtain from (2.2) and (2.3)

$$-\sum_{q \in N_p} \frac{u_q - u_p}{d_{pq}} m(e_{pq}) = 0, \quad (2.4)$$

which can be written in the form

$$\sum_{q \in u_p} \frac{m(e_{pq})}{d_{pq}} (u_p - u_q) = 0, \quad (2.5)$$

representing the linear system of algebraic equations for FVM. Then the term $\frac{m(e_{pq})}{d_{pq}}$ defined on sides of finite volume p is referred to as the transmissivity coefficient [5]. The system (2.5) must be accompanied by the boundary conditions. In case of the Dirichlet BC, we prescribe the value of u_q on the boundary. In case of the oblique derivative BC (1.2) it needs a special treatment which is discussed in the following subsections.

2.1. Oblique derivative BC - 2D case. In this section we are dealing with the numerical solution to the oblique derivative BVP (1.1)-(1.3) and we restrict our attention to 2D computational domain $\Omega \subset R^2$.

We have to suggest a method for discretization of (1.2). To that goal we consider a splitting of the gradient in normal and tangential directions

$$\nabla u = \langle \nabla u, \vec{n} \rangle \vec{n} + \langle \nabla u, \vec{t} \rangle \vec{t} = \frac{\partial u}{\partial \vec{n}} \vec{n} + \frac{\partial u}{\partial \vec{t}} \vec{t}, \quad (2.6)$$

where \vec{n} is the normal vector and \vec{t} is a tangent vector to Γ .

Now we put (2.6) into (1.2) and obtain

$$\langle \nabla u, \vec{s} \rangle = \left\langle \frac{\partial u}{\partial \vec{n}} \vec{n} + \frac{\partial u}{\partial \vec{t}} \vec{t}, \vec{s} \right\rangle = \frac{\partial u}{\partial \vec{n}} \langle \vec{n}, \vec{s} \rangle + \frac{\partial u}{\partial \vec{t}} \langle \vec{t}, \vec{s} \rangle. \quad (2.7)$$

Thus the condition (1.2) is transformed into

$$\frac{\partial u}{\partial \vec{n}} \langle \vec{n}, \vec{s} \rangle + \frac{\partial u}{\partial \vec{t}} \langle \vec{t}, \vec{s} \rangle = p. \quad (2.8)$$

Then we set as approximations of normal and tangent vectors,

$$\vec{n} = \left(\frac{x_{i-1,j} - x_{i,j}}{|\mathbf{x}_{i-1,j} - \mathbf{x}_{i,j}|}, \frac{y_{i-1,j} - y_{i,j}}{|\mathbf{x}_{i-1,j} - \mathbf{x}_{i,j}|} \right), \quad (2.9)$$

$$\vec{t} = \left(\frac{x_N - x_S}{|\mathbf{x}_N - \mathbf{x}_S|}, \frac{y_N - y_S}{|\mathbf{x}_N - \mathbf{x}_S|} \right), \quad (2.10)$$

where $\mathbf{x}_{i,j} = (x_{i,j}, y_{i,j})$ is a representative point of the finite volume $p = (i, j)$ and $\mathbf{x}_{i-\frac{1}{2},j} = (x_{i-\frac{1}{2},j}, y_{i-\frac{1}{2},j})$, $\mathbf{x}_N = (x_N, y_N)$ and $\mathbf{x}_S = (x_S, y_S)$ are points on the boundary Γ , see Figure 2.1. For the definition of the oblique vector \vec{s} in our numerical experiments we use a mass point source $\mathbf{x}_C = (x_C, y_C) \in R^2$ and we consider

$$\vec{s} = \left(\frac{x_C - x_{i-\frac{1}{2},j}}{|\mathbf{x}_C - \mathbf{x}_{i-\frac{1}{2},j}|}, \frac{y_C - y_{i-\frac{1}{2},j}}{|\mathbf{x}_C - \mathbf{x}_{i-\frac{1}{2},j}|} \right). \quad (2.11)$$

By $u_{i,j}$ we denote the approximate value of the solution u in the finite volume $p = (i, j)$. Then we approximate the normal and tangential derivatives in (2.8) by

$$\frac{\partial u}{\partial \vec{n}} = \frac{u_{i-1,j} - u_{i,j}}{|\mathbf{x}_{i-1,j} - \mathbf{x}_{i,j}|}, \quad (2.12)$$

$$\frac{\partial u}{\partial \vec{t}} = \frac{u_N - u_S}{|\mathbf{x}_N - \mathbf{x}_S|}, \quad (2.13)$$

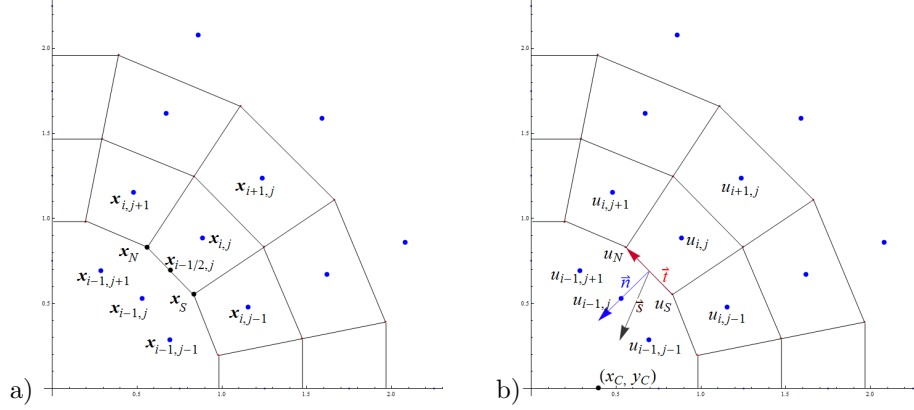


FIG. 2.1. Illustration of 2D FVM grid

where values u_S , u_N are defined by

$$u_N = \frac{u_{i,j} + u_{i,j+1} + u_{i-1,j} + u_{i-1,j+1}}{4},$$

$$u_S = \frac{u_{i,j} + u_{i,j-1} + u_{i-1,j} + u_{i-1,j-1}}{4},$$

and for the bottom boundary, i.e. $i = 1$, we add new unknowns which are then included into the system. If we put these approximations into (2.8), we get a discrete form of the 2D oblique derivative BC (1.2) in the form

$$\langle \nabla u, \vec{s} \rangle \approx \frac{u_{i-1,j} - u_{i,j}}{|\mathbf{x}_{i-1,j} - \mathbf{x}_{i,j}|} \langle \vec{n}, \vec{s} \rangle + \frac{u_N - u_S}{|\mathbf{x}_N - \mathbf{x}_S|} \langle \vec{t}, \vec{s} \rangle = p. \quad (2.14)$$

Our FVM for solving (1.1)-(1.3) then consist of solving system (2.5) for all inner finite volumes accompanied by the equations (2.14) for finite volumes along the bottom boundary Γ and by considering Dirichlet BC for finite volumes along $\partial\Omega - \Gamma$.

2.2. Oblique derivative BC - 3D case. In 3D case, we follow the similar strategy as in 2D case. To that goal, we split of the gradient in normal and two tangential directions

$$\nabla u = \langle \nabla u, \vec{n} \rangle \vec{n} + \langle \nabla u, \vec{t}_1 \rangle \vec{t}_1 + \langle \nabla u, \vec{t}_2 \rangle \vec{t}_2 = \frac{\partial u}{\partial \vec{n}} \vec{n} + \frac{\partial u}{\partial \vec{t}_1} \vec{t}_1 + \frac{\partial u}{\partial \vec{t}_2} \vec{t}_2, \quad (2.15)$$

where \vec{n} is the normal vector and \vec{t}_1 , \vec{t}_2 are linearly independent tangent vectors to $\Gamma \subset \partial\Omega \subset R^3$. As in 2D case, we put (2.15) into (1.2) to obtain

$$\langle \nabla u, \vec{s} \rangle = \langle \frac{\partial u}{\partial \vec{n}} \vec{n} + \frac{\partial u}{\partial \vec{t}_1} \vec{t}_1 + \frac{\partial u}{\partial \vec{t}_2} \vec{t}_2, \vec{s} \rangle = \frac{\partial u}{\partial \vec{n}} \langle \vec{n}, \vec{s} \rangle + \frac{\partial u}{\partial \vec{t}_1} \langle \vec{t}_1, \vec{s} \rangle + \frac{\partial u}{\partial \vec{t}_2} \langle \vec{t}_2, \vec{s} \rangle \quad (2.16)$$

and the BC (1.2) is transformed into the form

$$\frac{\partial u}{\partial \vec{n}} \langle \vec{n}, \vec{s} \rangle + \frac{\partial u}{\partial \vec{t}_1} \langle \vec{t}_1, \vec{s} \rangle + \frac{\partial u}{\partial \vec{t}_2} \langle \vec{t}_2, \vec{s} \rangle = p. \quad (2.17)$$

We set approximations of normal and tangent vectors

$$\vec{n} = \left(\frac{x_{i-1,j,k} - x_{i,j,k}}{|\mathbf{x}_{i-1,j,k} - \mathbf{x}_{i,j,k}|}, \frac{y_{i-1,j,k} - y_{i,j,k}}{|\mathbf{x}_{i-1,j,k} - \mathbf{x}_{i,j,k}|}, \frac{z_{i-1,j,k} - z_{i,j,k}}{|\mathbf{x}_{i-1,j,k} - \mathbf{x}_{i,j,k}|} \right), \quad (2.18)$$

$$\vec{t}_1 = \left(\frac{x_{EN} - x_{WS}}{|\mathbf{x}_{EN} - \mathbf{x}_{WS}|}, \frac{y_{EN} - y_{WS}}{|\mathbf{x}_{EN} - \mathbf{x}_{WS}|}, \frac{z_{EN} - z_{WS}}{|\mathbf{x}_{EN} - \mathbf{x}_{WS}|} \right), \quad (2.19)$$

$$\vec{t}_2 = \left(\frac{x_{WN} - x_{ES}}{|\mathbf{x}_{WN} - \mathbf{x}_{ES}|}, \frac{y_{WN} - y_{ES}}{|\mathbf{x}_{WN} - \mathbf{x}_{ES}|}, \frac{z_{WN} - z_{ES}}{|\mathbf{x}_{WN} - \mathbf{x}_{ES}|} \right), \quad (2.20)$$

where $\mathbf{x}_{i,j,k} = (x_{i,j,k}, y_{i,j,k}, z_{i,j,k})$ is a representative point of the finite volume $p = (i, j, k)$ and $\mathbf{x}_{i-\frac{1}{2},j,k} = (x_{i-\frac{1}{2},j,k}, y_{i-\frac{1}{2},j,k}, z_{i-\frac{1}{2},j,k})$, $\mathbf{x}_{WN} = (x_{WN}, y_{WN}, z_{WN})$, $\mathbf{x}_{EN} = (x_{EN}, y_{EN}, z_{EN})$, $\mathbf{x}_{WS} = (x_{WS}, y_{WS}, z_{WS})$ and $\mathbf{x}_{ES} = (x_{ES}, y_{ES}, z_{ES})$ are points on the bottom boundary Γ , see Figure 2.2. In our numerical experiments, we consider the oblique vector in the form

$$\vec{s} = \left(\frac{x_C - x_{i-\frac{1}{2},j,k}}{|\mathbf{x}_C - \mathbf{x}_{i-\frac{1}{2},j,k}|}, \frac{y_C - y_{i-\frac{1}{2},j,k}}{|\mathbf{x}_C - \mathbf{x}_{i-\frac{1}{2},j,k}|}, \frac{z_C - z_{i-\frac{1}{2},j,k}}{|\mathbf{x}_C - \mathbf{x}_{i-\frac{1}{2},j,k}|} \right), \quad (2.21)$$

where \mathbf{x}_C is the point $\mathbf{x}_C = (x_C, y_C, z_C) \in R^3$. By $u_{i,j,k}$ we denote the approximate

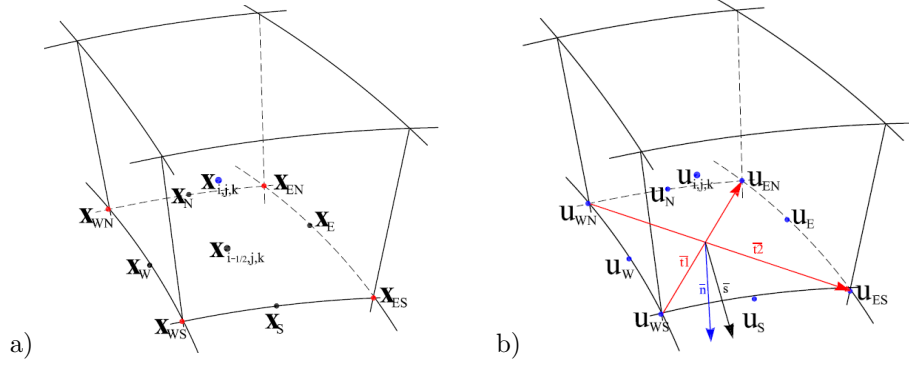


FIG. 2.2. Illustration of 3D FVM grid

value of the solution u in the finite volume $p = (i, j, k)$ and we approximate the normal and tangential derivatives in (2.17) by

$$\frac{\partial u}{\partial \vec{n}} = \frac{u_{i-1,j,k} - u_{i,j,k}}{|\mathbf{x}_{i-1,j,k} - \mathbf{x}_{i,j,k}|}, \quad (2.22)$$

$$\frac{\partial u}{\partial \vec{t}_1} = \frac{u_{EN} - u_{WS}}{|\mathbf{x}_{EN} - \mathbf{x}_{WS}|}, \quad (2.23)$$

$$\frac{\partial u}{\partial \vec{t}_2} = \frac{u_{WN} - u_{ES}}{|\mathbf{x}_{WN} - \mathbf{x}_{ES}|}, \quad (2.24)$$

where values u_{WN} , u_{EN} , u_{WS} , u_{ES} are defined by

$$\begin{aligned} u_{WN} &= \frac{u_{i,j,k} + u_{i,j-1,k} + u_{i,j,k-1} + u_{i,j-1,k-1} + u_{i-1,j,k} + u_{i-1,j-1,k} + u_{i-1,j,k-1} + u_{i-1,j-1,k-1}}{8}, \\ u_{EN} &= \frac{u_{i,j,k} + u_{i,j-1,k} + u_{i,j,k+1} + u_{i,j-1,k+1} + u_{i-1,j,k} + u_{i-1,j-1,k} + u_{i-1,j,k+1} + u_{i-1,j-1,k+1}}{8}, \\ u_{WS} &= \frac{u_{i,j,k} + u_{i,j+1,k} + u_{i,j,k-1} + u_{i,j+1,k-1} + u_{i-1,j,k} + u_{i-1,j+1,k} + u_{i-1,j,k-1} + u_{i-1,j+1,k-1}}{8}, \\ u_{ES} &= \frac{u_{i,j,k} + u_{i,j+1,k} + u_{i,j,k+1} + u_{i,j+1,k+1} + u_{i-1,j,k} + u_{i-1,j+1,k} + u_{i-1,j,k+1} + u_{i-1,j+1,k+1}}{8}. \end{aligned}$$

If we put these approximations into (2.17) we get a discrete form of the 3D oblique derivative BC (1.2)

$$\langle \nabla u, \vec{s} \rangle \approx \frac{u_{i-1,j,k} - u_{i,j,k}}{|\mathbf{x}_{i-1,j,k} - \mathbf{x}_{i,j,k}|} \langle \vec{n}, \vec{s} \rangle + \frac{u_{EN} - u_{WS}}{|\mathbf{x}_{EN} - \mathbf{x}_{WS}|} \langle \vec{t}_1, \vec{s} \rangle + \frac{u_{WN} - u_{ES}}{|\mathbf{x}_{WN} - \mathbf{x}_{ES}|} \langle \vec{t}_2, \vec{s} \rangle = p. \quad (2.25)$$

These equations are incorporated into the FVM linear system which is then solved.

3. Numerical experiments. In this section, we present several numerical experiments which were performed in order to test the proposed numerical schemes. In

2D experiments - Computational domains and boundary conditions				
Exp.	r	θ	Type of BCs	\mathbf{x}_C
1.	(1, 2)	(0, 2π)	Dirichlet - Neumann	—
2.	(1, 2)	(0, 2π)	Oblique with projection to normal	(0.3, -0.1)
3.	(1, 2)	(0, 2π)	Oblique	(-0.1, -0.3)
4.	(1, 2)	(0, 2π)	Oblique with rotation by 15°	(0.2, 0.4)
5.	(1, 2)	(0, $\frac{\pi}{4}$)	Oblique	(0.4, -0.3)

TABLE 3.1

2D experiments - Computational domains and types of boundary conditions; r and θ are polar coordinates and in column \mathbf{x}_C are cartesian coordinates of the mass point source.

3D experiments - Computational domains and boundary conditions				
Exp.	r	$\theta \times \phi$	Type of BCs	Center \mathbf{x}_C
1.	(1, 2)	$(0, \frac{\pi}{4}) \times (0, \frac{\pi}{4})$	Obl. with projection to normal	(-0.2, 0.1, 0.05)
2.	(1, 2)	$(0, \frac{\pi}{4}) \times (0, \frac{\pi}{4})$	Oblique	(-0.2, 0.1, 0.25)
3.	(1, 2)	$(0, \frac{\pi}{4}) \times (0, \frac{\pi}{4})$	Oblique with rotation by 15°	(0.3, -0.2, 0.1)

TABLE 3.2

3D experiments - Computational domains and types of boundary conditions; r , θ and ϕ are spherical coordinates and \mathbf{x}_C there are cartesian coordinates of the mass point source.

2D experiments, the computational domain has been the annulus between two circles and segment of this annulus, see Table 3.1. As the Dirichlet BC (1.3) on the upper boundary (in the *Exp. 5.* on the side boundaries as well) the values of exact solution of (1.1) (in the form $u(x, y) = -\ln r$, where r is the distance from the mass point source \mathbf{x}_C , i.e. $r = |\mathbf{x} - \mathbf{x}_C|$) have been applied. As the Neumann/oblique BC on the bottom boundary the derivative of this exact solution (which is equal to $1/r$ in radial direction) has been considered.

In 3D numerical experiments, the computational domain has been a tesseract defined in Table 3.2. The Dirichlet BC (1.3) in the form of the exact solution of (1.1) (i.e. $u(x, y, z) = 1/r$) has been applied on the upper and the side boundaries. As the Neumann/oblique BC on the bottom boundary the derivative of exact solution (equals to $-1/r^2$ in radial direction) has been applied.

The numerical results have been compared with the exact solution. In Tables 3.3-3.10 the $L_2(\Omega)$ -norm of differences between the exact and numerical solutions and EOC of the methods are presented. All experimental results show EOC=2 for the proposed methods.

3.1. 2D Case. In the first experiment we have considered combination of BCs, on the upper boundary the Dirichlet BC and on bottom boundary the Neumann BC, see Table 3.1. The point $\mathbf{x}_C = (0, 0)$. The results can be seen in Table 3.3 and Figure 3.1 a), EOC = 2. In these numerical experiments, the accuracy of solution

depends only on the splitting in radial direction, i.e., we refine the grid only in index i and j is arbitrary, see Table 3.3. Second experiment we tested an approach where

Combined boundary condition		
Grid	$\ \mathbf{u} - u\ _{L_2}$	EOC
$64 \times j$	$9.344708 \cdot 10^{-6}$	-
$128 \times j$	$2.281765 \cdot 10^{-6}$	2.034
$256 \times j$	$5.637187 \cdot 10^{-7}$	2.0171
$512 \times j$	$1.400943 \cdot 10^{-7}$	2.00858
$1024 \times j$	$3.492142 \cdot 10^{-8}$	2.00421

TABLE 3.3
 $L_2(\Omega)$ -norm and EOC for the 2D Exp 1. with standard Dirichlet - Neumann boundary condition.

the oblique vector \vec{s} is projected to the normal vector \vec{n}_Γ and the value $p \cos \theta$, $\theta = \angle(\vec{s}, \vec{n}_\Gamma)$ is considered as value of derivative in normal direction. This approach is correct if we know the direction of the gradient and $\vec{s} = \frac{\nabla u}{|\nabla u|}$. In this experiment, \mathbf{x}_C is shifted to $(0.3, -0.1)$. The $L_2(\Omega)$ -norm of differences between the exact and numerical solutions and EOC of the method are shown in Table 3.4. On the contrary with the previous experiments, now the accuracy of the solution depends on both coordinates and more substantially on the radial direction. In the third experiment,

Oblique boundary condition		
Grid	$\ \mathbf{u} - u\ _{L_2}$	EOC
4×8	$7.099696 \cdot 10^{-3}$	-
8×16	$1.875149 \cdot 10^{-3}$	1.92075
16×32	$4.6107913 \cdot 10^{-4}$	2.02392
32×64	$1.134551 \cdot 10^{-4}$	2.02289
64×128	$2.808830 \cdot 10^{-5}$	2.01408

TABLE 3.4
 $L_2(\Omega)$ -norm and EOC for the 2D Exp 2. with oblique derivative boundary condition when the oblique vector $\vec{s} = \frac{\nabla u}{|\nabla u|}$ is projected to normal vector \vec{n} with $\mathbf{x}_C = (0.3, -0.1)$.

we have considered the oblique BC (1.2) on the bottom boundary without projection to the normal but with splitting of the gradient to normal and tangential directions, $\mathbf{x}_C = (-0.1, -0.3)$. The result can be seen in Table 3.5 and in Figure 3.1 b). For the

Oblique boundary condition		
Grid	$\ \mathbf{u} - u\ _{L_2}$	EOC
8×16	$1.195339 \cdot 10^{-2}$	-
16×32	$2.846202 \cdot 10^{-3}$	2.07031
32×64	$6.893848 \cdot 10^{-4}$	2.04566
64×128	$1.693563 \cdot 10^{-4}$	2.02525
128×256	$4.193662 \cdot 10^{-5}$	2.01378

TABLE 3.5
 $L_2(\Omega)$ -norm and EOC for the 2D Exp 3. with oblique boundary condition experiment with $\mathbf{x}_C = (-0.1, -0.3)$.

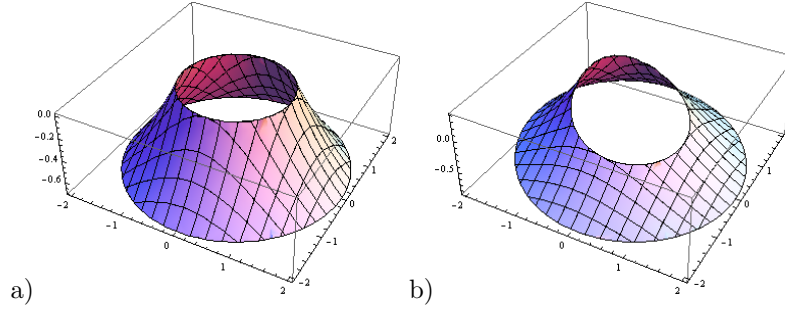


FIG. 3.1. Graph of the 2D solution a) Neumann and Dirichlet BC b) Oblique and Dirichlet BC on the bottom boundary

fourth numerical experiment we have the same BC as in the previous experiment, but the oblique vector \vec{s} has been given by rotation of \vec{s}_1 by 15° where \vec{s}_1 is the normalized gradient vector of the exact solution. The displacement of the mass source has been $\mathbf{x}_C = (0.2, 0.4)$. The $L_2(\Omega)$ -norm of differences between the exact and numerical solutions and EOC of the method are shown in Table 3.6. In the last numerical 2D

Oblique boundary condition		
Grid	$\ \mathbf{u} - u\ _{L_2}$	EOC
4×8	$3.035999 \cdot 10^{-2}$	-
8×16	$1.258422 \cdot 10^{-2}$	1.27056
16×32	$2.781355 \cdot 10^{-3}$	2.1777
32×64	$6.712759 \cdot 10^{-4}$	2.05081
64×128	$1.652955 \cdot 10^{-4}$	2.02186

TABLE 3.6

$L_2(\Omega)$ -norm and EOC for the 2D Exp 4. with oblique derivative boundary condition when the oblique vector \vec{s} does not have direction of the solution gradient.

experiment, see Table 3.1, we have considered the same oblique BC as in *Exp 3*. and on the side boundaries the Dirichlet BC has been applied. The $L_2(\Omega)$ -norm of differences between the exact and numerical solutions and EOC of the method for center point $\mathbf{x}_C = (0.4, -0.3)$ are shown in Table 3.7.

Oblique boundary conditions		
Grid	$\ \mathbf{u} - u\ _{L_2}$	EOC
4×4	$8.103634 \cdot 10^{-4}$	-
8×8	$1.331729 \cdot 10^{-4}$	2.60527
16×16	$2.564994 \cdot 10^{-6}$	2.37627
32×32	$5.556186 \cdot 10^{-6}$	2.20679
64×64	$1.289188 \cdot 10^{-6}$	2.10763

TABLE 3.7

$L_2(\Omega)$ -norm and EOC for the 2D Exp 5. oblique derivative boundary condition in experiment on the segment of annulus.

3.2. 3D Case. In the first 3D experiment, similarly to above discussed 2D case, the Dirichlet BC on the upper and planar boundaries has been considered and the Neu-

mann BC, where oblique vector \vec{s} is projected to normal vector \vec{n} on bottom boundary has been applied. The mass source has been $\mathbf{x}_C = (-0.2, 0.1, 0.05)$. The results can be seen in Table 3.8. In the second experiment, we have considered the oblique BC

Oblique boundary condition		
Grid	$\ \mathbf{u} - u\ _{L_2}$	EOC
$1 \times 1 \times 2$	$1.50876 \cdot 10^{-0}$	-
$2 \times 2 \times 4$	$8.89055 \cdot 10^{-2}$	4.08495
$4 \times 4 \times 8$	$1.18641 \cdot 10^{-2}$	2.90567
$8 \times 8 \times 16$	$2.02324 \cdot 10^{-3}$	2.55186
$16 \times 16 \times 32$	$3.90073 \cdot 10^{-4}$	2.37485

TABLE 3.8

$L_2(\Omega)$ -norm and EOC for the 3D Exp 1. oblique derivative boundary condition when the oblique vector \vec{s} is projected to normal vector \vec{n} with the mass center point $\mathbf{x}_C = (-0.2, 0.1, 0.05)$.

(1.2) treated by (2.25) on the bottom boundary and the Dirichlet BC on the upper and planar boundaries. The mass point center has been $\mathbf{x}_C = (-0.2, 0.1, 0.25)$. The result can be seen in Table 3.9. For the last 3D numerical experiment, we have the

Oblique boundary condition		
Grid	$\ \mathbf{u} - u\ _{L_2}$	EOC
$1 \times 1 \times 2$	$1.55421 \cdot 10^{-0}$	-
$2 \times 2 \times 4$	$8.37978 \cdot 10^{-2}$	4.21313
$4 \times 4 \times 8$	$1.04018 \cdot 10^{-2}$	3.01008
$8 \times 8 \times 16$	$1.62235 \cdot 10^{-3}$	2.68067
$16 \times 16 \times 32$	$2.81640 \cdot 10^{-4}$	2.52616

TABLE 3.9

$L_2(\Omega)$ -norm and EOC for the 3D Exp 2. oblique boundary condition experiment with the shifted center point $\mathbf{x}_C = (-0.2, 0.1, 0.25)$.

same BCs as in the previous experiment, but the oblique vector \vec{s} has been given by rotation of \vec{s}_1 around z -axis by 15° where \vec{s}_1 is the exact solution unit gradient vector. The displacement of the center point has been $\mathbf{x}_C = (0.3, -0.2, 0.1)$. The $L_2(\Omega)$ -norm of differences between the exact and numerical solutions and EOC of the method are shown in Table 3.10.

Oblique boundary condition		
Grid	$\ \mathbf{u} - u\ _{L_2}$	EOC
$1 \times 1 \times 2$	$1.93856 \cdot 10^{-0}$	-
$2 \times 2 \times 4$	$9.55366 \cdot 10^{-2}$	4.34279
$4 \times 4 \times 8$	$1.21764 \cdot 10^{-2}$	2.97196
$8 \times 8 \times 16$	$2.09633 \cdot 10^{-3}$	2.53815
$16 \times 16 \times 32$	$4.54241 \cdot 10^{-4}$	2.20634

TABLE 3.10

$L_2(\Omega)$ -norm and EOC for the 3D Exp 3. oblique derivative boundary condition when the oblique vector \vec{s} does not have direction of the solution gradient.

4. Conclusions. We have presented the novel algorithm for solving the oblique derivative boundary value problem by the finite volume method in 2D and 3D domains. In this approach, the oblique derivative in the boundary condition has been decomposed into normal and tangential components. The proposed 2D and 3D numerical schemes have been tested and numerical solutions have been compared with the exact solutions. All numerical experiments show that the proposed numerical scheme is second order accurate. In the near future, we would like to apply this scheme in the field of physical geodesy to solve the fixed gravimetric boundary value problem on the real Earth surface topography.

REFERENCES

- [1] R.BARRETT, M.BERRY, *Templates of the Solution of Linear System: Building Blocks for Iterative Methods - 2nd Edition*, Philadelphia, SIAM, (1994).
- [2] A.BRADJI, T.GALLOUT, *Error estimate for Finite volume approximate solutions of some oblique derivative boundary value problems*, International Journal On Finite Volumes, vol. 3, no 2, (2006).
- [3] R.ČUNDERLÍK, K.MIKULA, M.MOJZEŠ, *Numerical solution of the linearized fixed gravimetric boundary-value problem*, Journal of Geodesy, Vol. 82, No. 1 (2008), 15 - 29.
- [4] R.ČUNDERLÍK, K.MIKULA, R. ŠPIR, *Formulation of the Fixed Gravimetric BVP*, VII Hotine-Marussi Symposium on Mathematical Geodesy, International Association of Geodesy Symposia Volume 137 (2012), 227-231.
- [5] R.EYMARD, T.GALLOUET, R.HERBIN, *Finite Volume Methods*, Handbook of Numerical Analysis (2003).
- [6] Z.FAŠKOVÁ, R.ČUNDERLÍK, K.MIKULA, *Finite element method for solving geodetic boundary value problems*, Journal of Geodesy, Vol. 84, No. 2 (2010), 135 - 144.
- [7] Z.FAŠKOVÁ, *Numerical methods for solving geodetic boundary value problem*, PhD Thesis, SvF STU Bratislava, Slovakia, (2008).
- [8] P.HOLOTA, *Coerciveness of the linear gravimetric boundary-value problem and a geometrical interpretation*, Journal of Geodesy 71(10) (1997), 640 - 651.
- [9] P.HOLOTA, O.NESVADBA, *Model Refinements and Numerical Solutions of Weakly Formulated Boundary-Value Problems in Physical Geodesy*, Proceedings of VI Hotine-Marussi Symposium on Theoretical and Computational Geodesy, Springer Berlin Heidelberg, Part IV (2008), 320-326.
- [10] R.KLEES, *Loesung des fixen geodaetischen Randwertproblems mit Hilfe der Randelementmethode*, DGK. Reihe C., Nr. 382, Muenchen (1992).
- [11] R.KLEES, M. VAN GELDEREN, C. LAGE, C. SCHWAB, *Fast numerical solution of the linearized Molodensky problem*, Journal of Geodesy 75 (2001), 349 - 362.
- [12] K.R.KOCH, A.J.POPE, *Uniqueness and existence for the geodetic boundary value problem using the known surface of the earth*, Bull.Géod.,(1972) 46:467 - 476.
- [13] R.LEHMANN, *Solving geodetic boundary value problems with parallel computers*, Geodetic boundary value problems in view of the one centimeter Geoid, Lecture Notes in Earth Sciences vol 65, Springer, Berlin, (1997).
- [14] P.MEISSEL, *The Use of Finite Elements in Physical Geodesy*, Report 313, Geodetic Science and Surveying, The Ohio State University, (1981).
- [15] O.NESVADBA, P. HOLOTA, R.KLEES, *A direct method and its numerical interpretation in the determination of the Earths gravity field from terrestrial data*, Tregoning P, Rizos C (eds) Dynamic planet monitoring and understanding a dynamic planet with geodetic and oceanographic tools, IAG Symposium, Cairns, Australia, 22 - 26, August 2005, chap. 54, vol 130. Springer, Berlin, (2007), pp 370 - 376.
- [16] M.G.SIDERIS, K.P.SCHWARZ, *Solving Molodenskys series by fast Fourier transform techniques*, Bull Geod, (1986), 60:5163
- [17] C.C.TSCHERNING, *Collocation and least squares methods as a tool for handling gravity field dependent data obtained through space research techniques*, Hieber S., Guyenne T.D. (eds) On space oceanography, navigation and geodynamics European workshop. European Space Agency, (1978), pp 141149.